International Design Engineering Technical Conferences & Computers and Information in Engineering Conference
IDETC2018
July 17-20, 2006, Miami, Florida, USA

IDETC (DETC2018-85873)

DESIGN AND SIMULATION OF A NOVEL MECHANICAL POWER TAKE-OFF FOR A TWO-BODY WAVE ENERGY POINT ABSORBER

Xiaofan Li
Research Assistant, Department of Mechanical Engineering, Virginia Tech.
Blacksburg, VA, the United States

Chien-An Chen
Research Assistant, Department of Electrical and Computer Engineering, Virginia Tech.
Blacksburg, VA, the United States

Qiuchi Xiong
Research Assistant, Department of Mechanical Engineering, Virginia Tech.
Blacksburg, VA, the United States

Robert Parker
Professor, Department of Mechanical Engineering, Virginia Tech.
Blacksburg, VA, the United States

Lei Zuo
Professor, Department of Mechanical Engineering, Virginia Tech.
Blacksburg, VA, the United States

ABSTRACT

In this paper, a two-body self-react wave energy converter with a novel mechanical Power Take-off (PTO) is introduced. The PTO rectifies the mechanical motion and regulates the flow with a mechanism called Mechanical Motion Rectifier (MMR), which converts the reciprocating motion of the ocean wave into unidirectional rotation of the generator. The overall system is analyzed in both time and frequency domain. In time domain, the piecewise non-linear dynamic model of the MMR PTO is derived, and parameters that could significantly influence the MMR property is extracted. By building the model into WEC-Sim, a time domain wave energy converter (WEC) simulation tool, to simulate and evaluate the performance of the PTO. In addition, the system is modelled as a two-body vibration system for frequency domain analysis in order to further investigate and optimize the proposed wave energy converter. The tunable parameters within the system, including the equivalent mass, the equivalent damping coefficient, and the PTO stiffness, are discussed based on the criteria of maximization of the total output power. To verify the theoretical analysis, a bench test prototype is developed and tested on a hydraulic test machine. The experimental results in line with the derived model and can be used for reasonable estimation on the output power of the proposed system in real ocean conditions.

INTRODUCTION

During the past few decades, extracting energy from ocean wave to benefit human goods has become a popular topic [1]. According to the U.S. Department of Energy, the available wave energy resource along the United States alone is 2,640 TWh/year; nearly two-thirds of the 4,000 TWh of electricity used in the United States each year [2]. As roughly 40% of the population lives within 20km of the coast [3], reasonable adoption of the ocean wave energy could be real potential.

Among all the renewable energies, ocean wave energy outstands for its relatively low impact on the environment and high power densities [4]. However, similar to but even worse than the wind energy, the wave condition could change dramatically within several hours and the excitation is in sinusoid instead of constant, this feature of ever-changing condition of the ocean wave requires highly self-adaptive structure to be able to adjust with the wave and work effectively. In addition to that, the harsh environment of the ocean with corrosive and salinity water requires a robust system, which could survive such situation. In order to overcome all these obstacles, the most important task relies on the Power take-off (PTO), which is the mechanism of the WEC to extract energy from wave force and produce electricity [5].

Knowing the importance of PTO, researchers around the world have invented various prototypes and achieved reasonable outcomes. For example, R Henderson has developed a duck type of WEC named Pelamis in which he used a hydraulic PTO [6,7]; Falcao designed a hydraulic PTO with gas accumulators to store the pressure and improve the performance [8]; Elwood et al. has built a two body WEC with specially designed linear generator PTO, which constrained the permanent magnets with the buoy and the core with the cylinder [9]; Lejerskog et al. designed and tested a direct drive single body point absorber, which has a direct connecting structure between the buoy and the PTO using a rope and the system is optimized for maximization of the power [10]. Although these PTOs are well iterated and comprehensively studied, there are

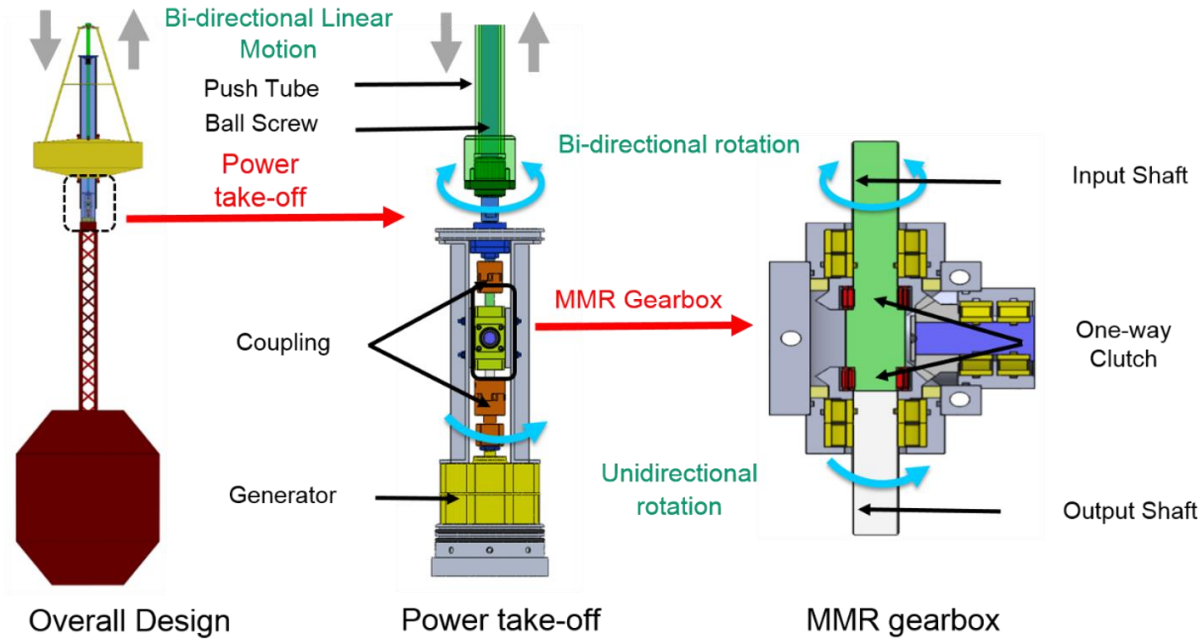

Figure.1 The design of WEC with MMR PTO

still some drawbacks preventing them from implementation. For instance, complexity of the hydraulic PTO could damage the reliability, and all the strictly sealed valves and accumulators could lead to large friction. In direct-drive PTO with the permanent magnetic generators, the reciprocating motion of the ocean wave causes the low speed actuation, and damages the overall efficiency of the PTO.

In this paper, the author first introduced a mechanism in PTO called Mechanical Motion Rectifier (MMR), which is able to rectify the bi-directional motion into unidirectional rotation to drive a permanent magnetic generator [11,12]. After the description for the design iteration, the dynamic model of proposed PTO is analyzed. Then the PTO is implemented into a two body wave energy point absorber type of WEC, both time-domain and frequency domain analysis for the overall system is introduced. At last, the proposed PTO is prototyped and tested as verification.

DESIGN OF THE MMR PTO

Figure.1 illustrates the design for the WEC with MMR PTO. The WEC consists of one floating buoy on the surface as the first body and one cylinder with a water tank submerged in the ocean as the second body. The cylinder will provide the space for the MMR PTO. The push tube at the top of the PTO is adopted to connect the relative motion between the two-body systems, and then the relative motion is transferred to the ball screw to convert the linear motion into rotation motion. Through some couplings, the bi-directional rotation motion is directed to the MMR gearbox where the motion is rectified. The MMR gearbox consists of one input shaft, one output shaft, three bevel gears, and two one-way clutches which only allow one-directional rotation and lock the contrary. The one-way clutches are inserted between the bevel gears and the input shaft. When the input rotation motion is in clockwise direction, the top one-way clutch disengages and the bottom one engages. The input motion isdirectly transferred to the output shaft. However, when the input motion is in counter-clockwise direction, the top one-way clutch engages and the bottom one disengages. The three bevel gears change the direction of the motion so the output will still in clockwise directional rotation. Through this mechanism, the motion of the input is rectified and the output will always rotate in one direction. This mechanism will benefit the PTO system through several aspects. Firstly, the motion of the system output is rectified into uni-direction, so the generator will always rotate in one direction, which will simplify the circuit for rectifying the electric current; secondly, the special mechanism of engage and disengage of the MMR will allow the generator continually working at low input speed which will help the generator to avoid the low efficiency zone at the very low speed; lastly yet importantly, the direct-drive PTO will simplify the structure of the PTO and bring advantage for maintaining and long-term reliability.

DYNAMIC OF THE MMR PTO

Figure.2 shows the diagram of the MMR PTO. where,

F_{pto} is the force of the PTO system,

$\dot{x}_{in}$ is the input linear motion speed to the ball screw,

ω_{in} is the input rotation speed to MMR gearbox,

ω_{out} is the output rotation speed from MMR gearbox,

T_{ge} is the torque from the generator,

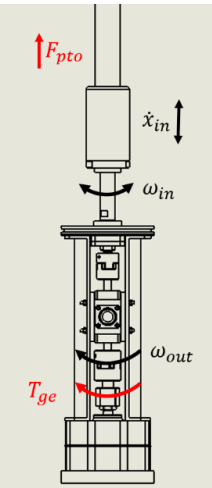

Figure.2 The scheme of the PTO

The relationship between ω_{in} and $\dot{x}_{in}$ can be introduced as:

$$\omega_{in} = \frac{2\pi \dot{x}_{in}}{l_{lead}}$$

Where l_{lead} is the lead length of the ball screw, indicating the ball screw will revolute one turn when each time the ball screw nut goes through that length.

The torque on the generator can be expressed as:

$$T_{ge} = \frac{\omega_{out} k_e k_t}{(R_{in} + R_{ex})}$$

Here,

k_e is the electric constant of the generator, denoting the ratio between the generator rotation speed and the output voltage,

k_t is the torque constant of the generator, denoting the ratio between the electric current on the generator and the torque on the generator,

R_{in} is the inner resistance of the generator,

R_{ex} is the external resistance of the generator.

Knowing the torque on the generator, the equivalent damping coefficient of the generator c_e can be derived through equality of input and output power:

$$c_e = \frac{k_e k_t}{(R_{in} + R_{ex})} \frac{4\pi^2}{l_{lead}^2}$$

When the MMR gearbox is engaged, in other words, $\omega_{in} = \omega_{out}$, the output speed of the MMR gearbox is the same with the input speed, the whole PTO work as an overall system and the system equation can be written as:

$$(m_{bs} + m_e)\ddot{x}_{in} + c_e \dot{x}_{in} = F_{pto}$$

Here,

m_{bs} is the mass of the ball screw,

m_e is the equivalent mass of the generator,

This condition is named as the "engaged" condition, where the overall system could be described in one equation.

However, when the output speed of the MMR gearbox is larger than that of the input speed, $\omega_{in} < \omega_{out}$, the overall system will be decoupled into two subsystems: one is the ball screw driven by the PTO force, another is the generator powering itself with the moment of inertia stored in the equivalent mass. The equations is then written as:

$$\begin{cases} m_{bs}\ddot{x}_{in} = F_{pto} \\ m_e \dot{\omega}_{out} + c_e \omega_{out} = 0 \end{cases}$$

This condition is named as the "disengaged" condition, where the both one-way clutch is disengaged and the generator is decoupled from the PTO system, the stored energy from the inertia of the generator will power the generator at certain speed to not die down to zero.

Figure.3 shows the simulation results for both the MMR PTO and the common linear PTO. When the system is disengaged, the input force required from the damping term, which is the generator, becomes zero. The output power is still larger than zero, indicating that the MMR should have larger power output with smaller input.

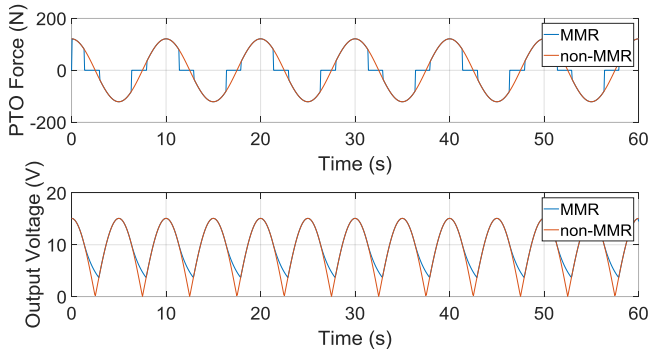

Figure.3 The scheme of the PTO

Knowing that the disengagement of the MMR PTO could benefit the overall energy harvesting effect of the system, the factor that could influence this unique character of the MMR system need to be explored. When the system is disengaged, solving the equation for the decoupled subsystem of the generator, the output speed can be acquired as:

$$\omega_{out} = e^{kt}$$
$$k = -\frac{c_e}{m_e}$$

This equation shows that the subsystem of the generator will die down exponentially with the constant k. Assuming the MMR PTO is under an excitation of a sinusoid input with angular velocity of ω, when disengage happens the rotation velocity is ω_0 and the time is t_0. Choosing Δt as infinite small, the equation for the time when system starts to disengage can be written as:

$$\omega_0 \sin(\omega(t_0 + \Delta t)) = \omega_0 \sin(\omega t_0)\, e^{k\Delta t}$$

Using trigonometric expansion for the left side of the equation, it becomes,

$$\omega_0 (\sin(\omega t_0)\cos(\omega \Delta t) + \sin(\omega \Delta t)\cos(\omega t_0)) = \omega_0 \sin(\omega t_0)\, e^{k\Delta t}$$

When $\Delta t \to 0$, the following relationship exist that $\cos(\omega \Delta t) = 1$, $\sin(\omega \Delta t) = \omega \Delta t$, the equation can be than written as:

$$1 + \omega \Delta t \cot(\omega t_0) = e^{k\Delta t}$$

By using Taylor expansion for $\Delta t \to 0$,

$$e^{k\Delta t} = 1 + k\Delta t + \frac{(k\Delta t)^2}{2!} + \frac{(k\Delta t)^3}{3!} + \cdots$$

Plug the expansion back into the original equation and ignore the high order infinite small terms, the time t_0 when the disengagement occur is:

$$t_0 = \frac{1}{\omega}\left(\frac{\pi}{2} - arctan\left(\frac{c_e}{m_e\omega}\right)\right)$$

This result indicates that the equivalent damping coefficient of the generator , the equivalent mass of the generator , and the excite frequency are the three main factors that could influence the disengagement character of the system. The simulation result for the disengage ratio, which is the time factor the disengagement occupied in one excite period, with different parameters in Figure.4shows that choosing a larger equivalent mass, a smaller equivalent damping coefficient, or a higher excitation frequency could help the system to get a larger disengage ratio.

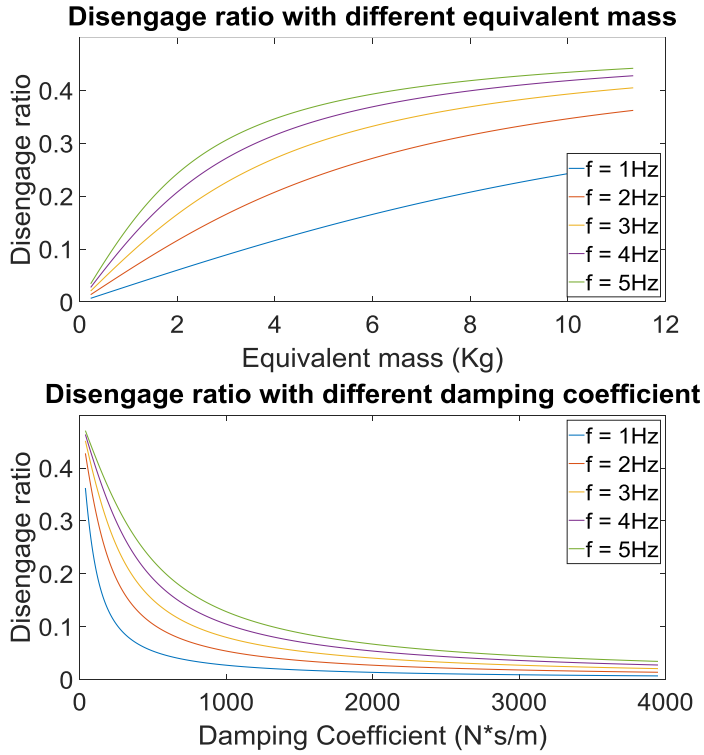

Figure.4 The influence of the equivalent mass and damping coefficient for the disengage ratio

DESIGN OF THE MMR PTO

With the dynamic property analyzed in the previous section, the dynamic analysis for the overall system requires further discussion. For the previous section only covers the dynamic property for the MMR PTO itself, the uniqueness of the MMR PTO could bring the overall system with unexpected outcome. The overall system is firstly analyzed in time domain using a time domain solver called WEC-Sim, which is developed by the NREL and the Sandia Nation Lab, to verify the dynamic model built for the MMR PTO [13]. Figure.5 illustrates model built into MATLAB Simulink for the WEC-Sim analysis. Since the MMR PTO has a piecewise nonlinear property, a separate block is used for describing the correct dynamic property of MMR PTO when the generator has been coupled/decoupled to the system. In addition to that, all the frequency dependent hydro-parameters has been included in the Simulink model so the real time simulation is reasonable. These parameters are obtained from the commercial software WAMIT, which uses the BEM to calculated the excitation force, added mass, and radiation damping of the system. Figure.6 shows the frequency dependent parameters mentioned above from WAMIT [14].

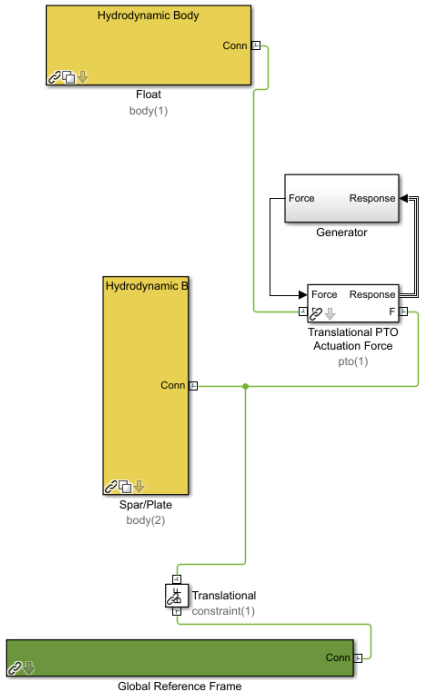

Figure.5 The Simulink model for the WEC-Sim analysis

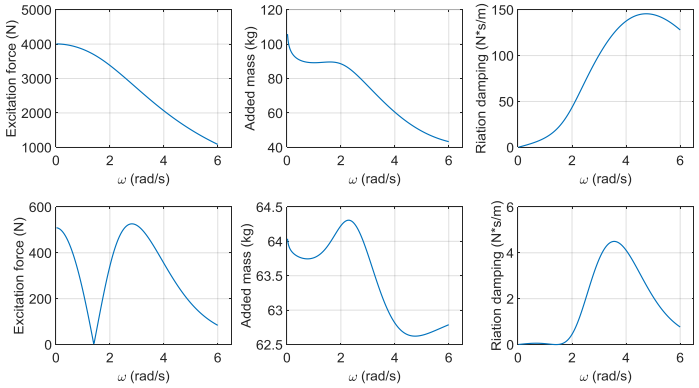

Figure.6 The hydro-parameters for the designed WEC

Figure.7 showed the time domain simulation results of the overall system with different equivalent mass under the same

wave excitation. It is easy to observe that under the given excitation condition, with the existing equivalent mass, there is no disengagement happened, however.When the equivalent mass is 20 times larger, the disengagement effect becomes obvious, proofing the previous analysis about the MMR PTO. However, it is also obvious that the output power becomes smaller with a larger equivalent mass, although the larger equivalent mass could increase the disengage ratio. The equivalent mass still demands further analysis and optimization for a better performance.

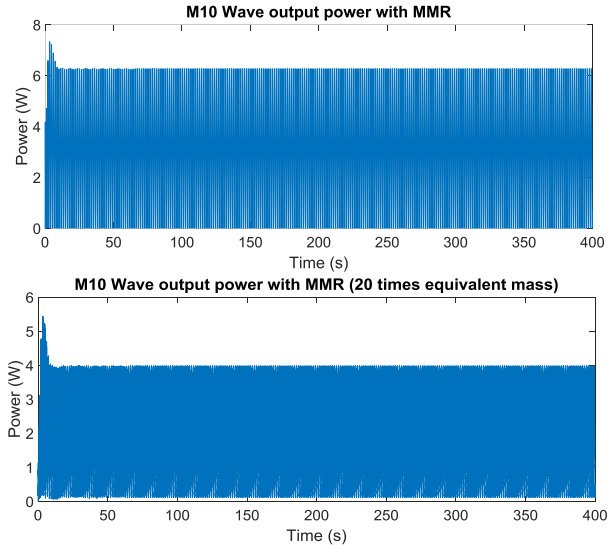

Figure.7 The time domain simulation results with different equivalent mass

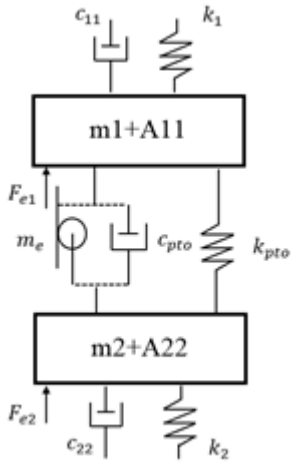

Figure.8 The scheme of the WEC

As a consequence, the scheme of overall system is shown in Figure.8. with the disengage ratio of the MMR PTO with different parameters obtained. By assuming that the PTO has a very small influence on the dynamic of the two body system, the system is schemed as linear and the benefit of the MMR PTO will be compensated later with the factor of disengage ratio. The equations of motion of the proposed self-reacting wave energy converter oscillating in heave can be derived through the scheme as:

$$(m_1 + A_{11})\ddot{x}_1 + m_e(\ddot{x}_1 - \ddot{x}_2) + c_{11}\dot{x}_1 + c_{pto}(\dot{x}_1 - \dot{x}_2) + k_1 x_1 + k_{pto}(x_1 - x_2) = f_{e1}$$

$$(m_2 + A_{22})\ddot{x}_2 + m_e(\ddot{x}_2 - \ddot{x}_1) + c_{22}\dot{x}_2 + c_{pto}(\dot{x}_2 - \dot{x}_1) + k_2 x_2 + k_{pto}(x_2 - x_1) = f_{e2}$$

Here, with the assumption that all the hydro parameters generated from the interference between the two bodies are relatively small and can be ignored, this assumption come from the observation of the results obtained from WAMIT, the ignored terms are in the scale of 0.01 compared with other terms:

x_1 and x_2 are the displacement of the floating and submerged body respectively

m_1 and m_2 are the mass of the floating and submerged body respectively

A_{11} and A_{22} are the frequency dependent added mass of the floating and submerged body respectively

c_{11} and c_{22} are the frequency dependent radiation damping of the floating and submerged body respectively

$c_{pto} = c_e$ is the equivalent damping coefficient of the generator

k_{pto} is the equivalent stiffness of the PTO

The system equation is then written in frequency domain for a close form solution, assuming the system is excited to a steady state under regular wave. The second body is submerged much deeper than the half length of the wave, so the excitation force cast on the second body is small and can be ignored, the system is rewritten with the assumption that $f_{e1} = F_1 e^{i\omega t}$, $f_{e2} = F_2 e^{i\omega t}$, $x_1 = X_1 e^{i\omega t}$, $x_2 = X_2 e^{i\omega t}$:

$$-\omega^2 AX + i\omega CX + KX = F$$

Where,

$$A = \begin{bmatrix} m_1 + m_e & -m_e \\ -m_e & m_2 + m_e \end{bmatrix},$$

$$C = \begin{bmatrix} c_{11} + c_{pto} & -c_{pto} \\ -c_{pto} & c_{22} + c_{pto} \end{bmatrix},$$

$$K = \begin{bmatrix} k_1 + k_{pto} & -k_{pto} \\ -k_{pto} & k_2 + k_{pto} \end{bmatrix},$$

$$X = \begin{bmatrix} X_1 \\ X_2 \end{bmatrix}, F = \begin{bmatrix} F_1 \\ F_2 \end{bmatrix}$$

The equation can be rewritten as:

$$X = (-\omega^2 A + i\omega C + K)^{-1} F$$

Define:

$$Z(i\omega) = -\omega^2 A + i\omega C + K = \begin{bmatrix} Z_{11} & Z_{12} \\ Z_{21} & Z_{22} \end{bmatrix}$$

And the expanded form is:

$$\begin{cases} Z_{11} = -\omega^2(m_1 + m_e) + i\omega(c_{11} + c_{pto}) + k_1 + k_{pto} \\ Z_{12} = \omega^2 m_e - i\omega c_{pto} - k_{pto} \\ Z_{21} = \omega^2 m_e - i\omega c_{pto} - k_{pto} \\ Z_{22} = -\omega^2(m_2 + m_e) + i\omega(c_{22} + c_{pto}) + k_2 + k_{pto} \end{cases}$$

The solution of the equation can be expressed as:

$$X_1 = \frac{Z_{22}F_1 - Z_{21}F_2}{\det(Z)}, X_2 = \frac{Z_{11}F_2 - Z_{12}F_1}{\det(Z)}$$

Knowing the solution to the system equations, the power absorbed from the ocean can be written as:

$$P_{pto} = \frac{1}{2}\omega^2 c_{pto}|X_1 - X_2|^2$$

By expanding the equation of the close form solution,

$$P_{pto} = \frac{1}{2}\omega^2 c_{pto}\left|\frac{p+iq}{(a+ib)m_e + (c+id)c_{pto} + (e+if)k_{pto} + g + ih}\right|^2$$

Where,

$$\begin{cases} p = k_2F_1 - k_1F_2 - \omega^2(m_2 + A_{22})F_1 + \omega^2(m_1 + A_{11})F_2 \\ q = \omega c_{22}F_1 - \omega c_{11}F_2 \\ a = \omega^4(m_1 + m_2) - \omega^2(k_1 + k_2) \\ b = -\omega^3(c_{11} + c_{22}) \\ c = \frac{b}{\omega} \\ d = -\frac{a}{\omega} \\ e = -\frac{a}{\omega^2} \\ f = -\frac{b}{\omega^2} \\ g = \omega^4 m_1 m_2 - \omega^2(m_1k_2 + m_2k_1) + k_1k_2 \\ h = -\omega^3(m_2c_{11} + m_1c_{22}) + \omega(k_2c_{11} + k_1c_{22}) \end{cases}$$

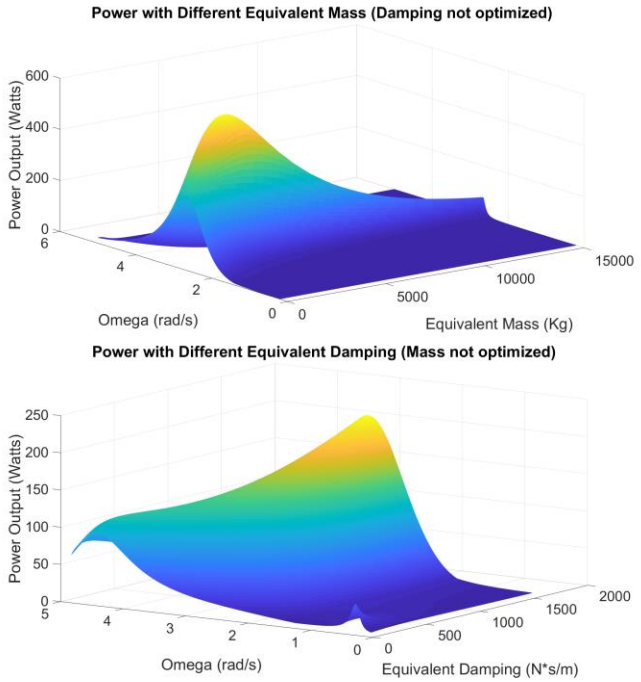

Figure.9 The output power with different equivalent mass and different damping coefficient

The mass ratio between the first body and the second body will also influence the outcome of the results, however, there exists plenty of literature explaining that and in this paper the ratio is set as constant of 10 times [15-17]. Accordingly, since the system is a rigid system, the PTO stiffness is also taken as constantly being zero. Figure.9(a) illustrates the power output for the WEC with a different excitation frequency and equivalent mass, whereas the Figure.9(b) shows the results under different excitation frequencies and damping coefficients.

The simulation results illustrated in Figure.9 indicate that both the parameter of equivalent mass and damping can have a large impact on the output of the WEC, so the system need to be optimized with respect to these two parameter.

By taking the partial derivative of the c_{pto} and m_e for the power output of the system:

$$(P_{pto})'_{c_{pto}} = \frac{0.5\omega^2(p^2+q^2)\left((bm_e+h)^2 + (am_e+g)^2 - (c^2+d^2)c_{pto}^2\right)}{\left((am_e + cc_{pto} + g)^2 + (bm_e + dc_{pto} + h)^2\right)^2}$$

$$(P_{pto})'_{m_e} = \frac{\omega^2 c_{pto}(p^2+q^2)\left((a^2+b^2)m_e + (ac+bd)c_{pto} + (ag+bh)\right)}{\left((am_e + cc_{pto} + g)^2 + (bm_e + dc_{pto} + h)^2\right)^2}$$

Let the two partial derivatives become zero:

$$(a^2+b^2)m_e + (ac+bd)c_{pto} + (ag+bh) = 0$$
$$(bm_e+h)^2 + (am_e+g)^2 - (c^2+d^2)c_{pto}^2 = 0$$

From the previous assumptions, it is easy to get an additional condition that:

$$ac + bd = 0$$

Plugging in this condition and solve the partial derivatives:

$$m_{eopt} = -\frac{ag+bh}{a^2+b^2}$$

$$c_{ptoopt} = \sqrt{\frac{(a^2+b^2)m_e^2 + (h^2+g^2) + 2(ag+bh)m_e}{c^2+d^2}}$$

The c_{ptoopt} can be simplified by using the condition that$(a^2+b^2) = (c^2+d^2)\omega^2$, the equation become:

$$c_{ptoopt} = \frac{|ah - bg|}{\omega(c^2+d^2)}$$

Knowing the c_{ptoopt} and m_{eopt}, the Hessian Metrix is checked for the derived equations to guarantee that the results obtained is the optimum condition instead of a saddle point.

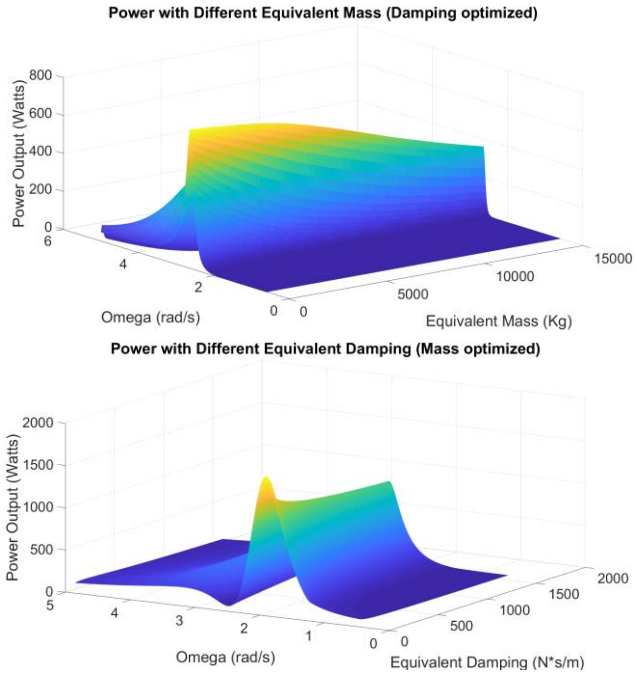

Figure.10 The output power with optimized damping coefficient for different equivalent mass and optimized equivalent mass for different damping coefficient

Figure.10 illustrates the simulation results of the power output with the calculated optimum condition, each point in the figure is with the optimized parameters. Figure.10 (a) showed the results for the output power with different equivalent mass and different frequency, the equivalent damping is optimized for the optimum output. Figure.10 (b) showed the results for the output power with different equivalent damping coefficient and different frequency, the equivalent mass is optimized similarly.

There remain two issues needed for further explanation on Figure.10, one is that the optimum frequency is mainly decided by the mass ratio between the first body and second body of the system, the author will not discuss this in detail here. The other is that it can be observed that the output power on Figure.10(b) is much larger. The reason is that in these cases, the numerically optimized equivalent mass is negative mass which will bring the energy to the system instead of capturing energy with the relative motion between the two bodies. However, the optimized damping coefficient are all positive, so the real world case should use the results in Figure.10(a) as the optimum condition rather than Figure.10(b).

With the optimum condition for linear PTO acquired, the optimum for the MMR system is then desired. However, due to the nonlinear property of the MMR PTO, there is no close form solution for the optimum. Numerical approach is used instead for the MMR PTO, the numerical simulation results are shown in Figure.11 indicating that the MMR system can have an advantage over the linear PTO on the power absorption.

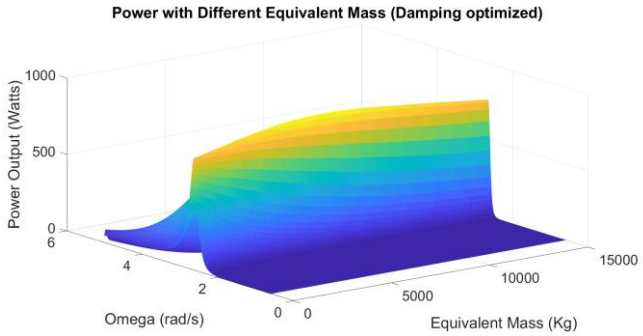

Figure.11 The output power with optimized damping coefficient for different equivalent mass considering the disengagement of the MMR PTO

BENCH TEST OF THE MMR PTO

In order to verify the simulation results and prove the advantage of having MMR as PTO, the purposed PTO was tested in lab with an Instron8801 hydraulic test machine. Figure.12 shows the fabricated PTO that is specifically designed for the bench test, the ball screw working in the bench test prototype has shorter stroke to fit the limit of the test machine, in addition to that, the adaptors and couplings are also modified to accommodate the space of the test machine.

Figure.12 The bench test prototype

Figure.13 illustrates the figure for the bench test, the prototype is assembled inside an aluminum cylinder and mounted upside down on a plate that is locked on the top of the test machine. The push rod of the PTO is actuated by the hydraulic actuator at the bottom of the test machine. The actuator will provide a base excitation to the PTO. The sensor embedded in the test machine measures the input force, the displacement to the PTO, and the voltage output of the generator through connecting the electric load to the generator. All the signals are recorded by the DAQ system of the Instron

Machine. Each phase of the generator is connected to an outer resistor with equivalent resistance and they are wired as Y type.

Figure.13 The developed prototype on the test machine

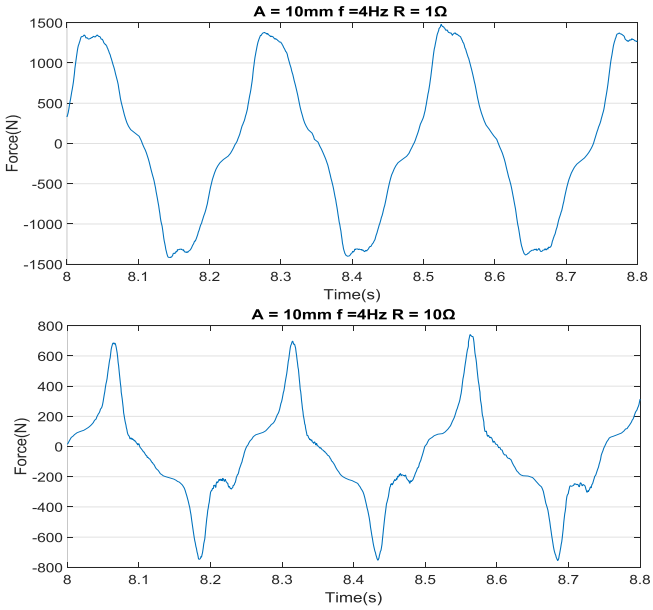

Figure.14 The actuation force for the MMR PTO with different outer resistance

Fig.14 shows the test result of actuator provided force of the MMR system under 10mm displacement, 4Hz base excitation. According to the previous simulation results, when the outer resistance is larger, the equivalent disengaged electric damping is smaller; leading to a more obvious disengagement, reflecting on the figure is the part where the PTO force is approaching level. However, due to the friction of the system, when the disengagement happens, the force on the system will be larger than zero and forms a stage shape in the time-force figure. When the MMR is engaged, the force from the generator will be non-zero again and drive the system in the regular sinusoid wave. It is clearly shown in the time-force plot that with the larger outer resistance, the ratio of disengagement time occupied in a full cycle is larger, which is consistent with the simulation results.

On the contrary, Figure.15 shows the force results between the MMR system and non-MMR system. It is easy to observe that under the same excitation, the shape of the force is different from each other. As explained above, for the MMR system, the disengage property and the friction force are the dominant force. However, due to the high frequency of the reciprocate motion and the backlash in the system, there exist an impact force at the beginning of each cycle, which is easy to observe from the figure and will significantly influence the force response of the non-MMR system.

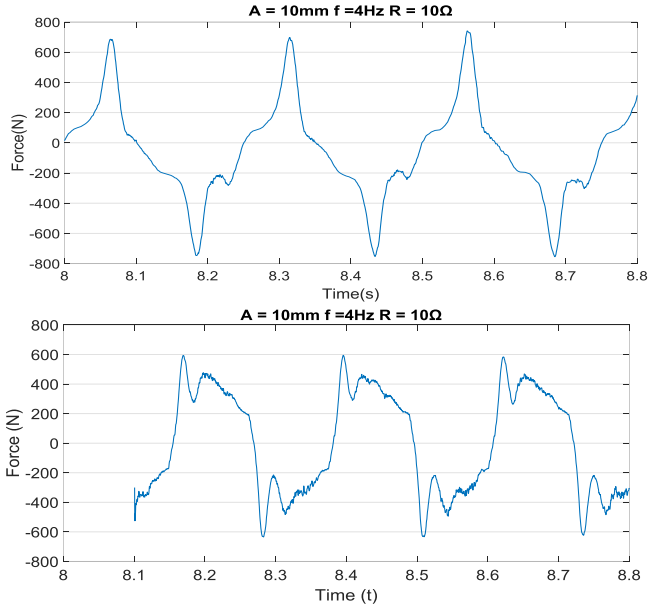

Figure.15 The actuation force for the MMR PTO with different outer resistance

Figure.16 shows two sets of test results for the efficiency of the proposed MMR PTO. The test condition is under sinusoid base excitation and the displacement for each set of test is set as 10mm. The base excitation displacement, the test damping coefficient and the equivalent mass is set to be the same and the test frequency is different. As predicted in the dynamic model, when the excitation frequency increases, the disengaged time section in each period will be longer. Thus the total energy harvesting efficiency will be higher.

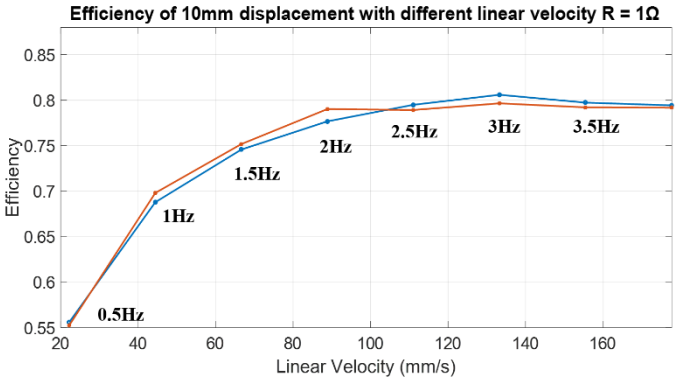

Figure.16 Efficiency results for the MMR PTO with different excitation frequency

In order to further prove the influence of the equivalent mass of the system as simulated above, flywheels has been made to adjust the equivalent mass of the MMR PTO. Figure.17 illustrates the MMR PTO with flywheel embeded. The flywheel is locked on the side shaft of the gearbox to contribute to the overall equivalent mass of the system.

Figure.17 The MMR PTO with flywheel to increase equivalent mass

Figure.18 illustrates the output of the generator with different flywheel added to the MMR system. Since the three phase PMG is wired in Y shape, the output on each phase was recorded individually. In order to prevent the test machine from overloading, one current signal has to be connected with the DAQ system of the test machine hence only two current signal was included in the result. In the figure, V_{ab}, V_{ac} and V_{bc} are the voltage output on each phase of the generator, I_a and I_b are the current output on two phase of the generator. The test condition is 10mm of displacement. 4Hz and the outer resistance on each phase is 10 ohms. The two flywheels each has a moment of inertia of 0.0049Kg*m^2 and 0.0098Kg*m^2.

It is easy to observe from the figure that for the MMR system with no flywheel, during each cycle, the voltage on each phase will go down to almost zero, indicating that the energy stored on the inertia of the generator is consumed by the electric damping of the generator, similarly, the current result also go down to zero. However, when the flywheel is added to the system, the inertia could store more energy, thus the generator could continue to work for longer time when the system is disengaged. Reflecting on the figure is that the voltage and current does not decrease to zero for the system with flywheel of 0.0049Kg*m^2, and the output voltage and current is almost constant with flywheel of 0.0098Kg*m^2. Indicating that the equivalent mass can play a very important role on the performance of the MMR PTO thus requires optimization. One noticeable condition is that the excitation frequency on the test machine is a lot higher than that of the ocean, so for the real ocean implementation the equivalent mass ratio of the flywheel will need further increased to reach the same disengage ratio showed in the bench test result.

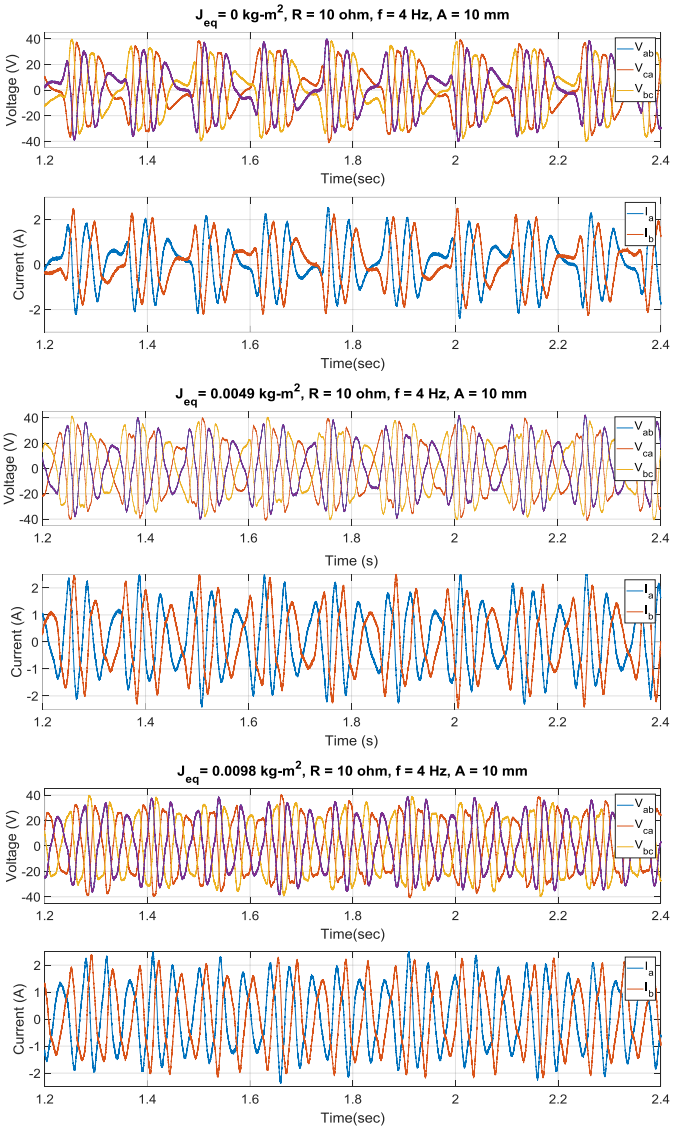

Figure.18 The generator output for MMR PTO with different equivalent mass

CONCLUSION

In this paper, the author designed and developed a two body wave point absorber with a novel PTO, the PTO uses a mechanism named MMR which can rectify the bi-directional rotation motion into uni-directional rotation, gaining the system with the advantage on both diminishing the force input and enlarging the power output. Dynamic model for both the PTO and the overall system is built, and the two most important factor, the equivalent mass and equivalent damping coefficient, that could influence the energy harvesting performance of the WEC is discussed and optimized accordingly. In addition to that, a bench test prototype developed based on the design verifies the theoretical model as well as the simulation results, and proofs the advantages of the MMR PTO.

ACKNOWLEDGMENTS

The author would like to acknowledge the U.S. Department of Energy (DOE) and National Science Foundation (NSF) for the funding opportunity. The author also would like to give acknowledgement to the undergraduate students David Kennedy, Rachael Chase and Rachael Duke who helped the topic during their independent study.

REFERENCES

[1]. Antonio, F. de O. "Wave energy utilization: A review of the technologies." *Renewable and sustainable energy reviews*14.3 (2010): 899-918.

[2]. Jacobson, Paul T., George Hagerman, and George Scott. *Mapping and assessment of the United States ocean wave energy resource*. No. DOE/GO/18173-1. Electric Power Research Institute, 2011

[3]. Huckerby, Jhon, et al. "An international vision for ocean energy." *The Ocean Energy Systems Implementing Agreement (OES)* (2011).

[4]. Chakrabarti, Subrata Kumar. *Hydrodynamics of offshore structures*. WIT press, 1987.

[5]. Falnes, Johannes. *Ocean waves and oscillating systems: linear interactions including wave-energy extraction*. Cambridge university press, 2002.

[6]. Henderson, Ross. "Design, simulation, and testing of a novel hydraulic power take-off system for the Pelamis wave energy converter." *Renewable energy* 31.2 (2006): 271-283.

[7]. Yemm, Richard, et al. "Pelamis: experience from concept to connection." *Phil. Trans. R. Soc. A* 370.1959 (2012): 365-380.

[8]. Ricci, P., et al. "Control strategies for a simple point-absorber connected to a hydraulic power take-off." *Proceedings of 8th European Wave and Tidal Energy Conference, Uppsala, Sweden*. 2009.

[9]. Elwood, David, et al. "Design, construction, and ocean testing of a taut-moored dual-body wave energy converter with a linear generator power take-off." *Renewable Energy* 35.2 (2010): 348-354.

[10]. Lejerskog, Erik, et al. "Experimental results on power absorption from a wave energy converter at the Lysekil wave energy research site." *Renewable energy* 77 (2015): 9-14.

[11]. Li, Zhongjie, et al. "Energy-harvesting shock absorber with a mechanical motion rectifier." *Smart Materials and Structures*22.2 (2012): 025008.

[12]. Liang, Changwei, Junxiao Ai, and Lei Zuo. "Design, fabrication, simulation and testing of an ocean wave energy converter with mechanical motion rectifier." *Ocean Engineering* 136 (2017): 190-200.

[13]. Lawson, Michael, et al. "Development and demonstration of the WEC-Sim wave energy converter simulation tool." (2014).

[14]. WAMIT. (2016) User Manual V7.2. WAMIT, Inc., Massachusetts.

[15]. Beatty, Scott J., et al. "Experimental and numerical comparisons of self-reacting point absorber wave energy converters in regular waves." *Ocean Engineering* 104 (2015): 370-386.

[16]. Falnes, Jonathan. "Wave-energy conversion through relative motion between two single-mode oscillating bodies." *Journal of Offshore Mechanics and Arctic Engineering* 121.1 (1999): 32-38.

[17]. Korde, Umesh A. "Systems of reactively loaded coupled oscillating bodies in wave energy conversion." *Applied ocean research* 25.2 (2003): 79-91.

